Article

Nonlinear Optical Properties of Zn(II) Porphyrin, Graphene Nanoplates, and Ferrocene Hybrid Materials

Francesca Limosani [1], Francesca Tessore [2],*, Alessandra Forni [3], Angelo Lembo [1], Gabriele Di Carlo [2], Cecilia Albanese [2], Stefano Bellucci [4] and Pietro Tagliatesta [1]

[1] Department of Chemical Science and Technologies, University of Rome "Tor Vergata", Via della Ricerca Scientifica 1, 00133 Rome, Italy; francesca.limosani@uniroma2.it (F.L.); angelo.lembo@uniroma2.it (A.L.); pietro.tagliatesta@uniroma2.it (P.T.)

[2] Department of Chemistry, University of Milan, Via C. Golgi 19, 20133 Milan, Italy; gabriele.dicarlo@unimi.it (G.D.C.); cecilia.albanese@unimi.it (C.A.)

[3] CNR-SCITEC, Istituto di Scienze e Tecnologie Chimiche "G. Natta", Via Golgi 19, 20133 Milan, Italy; alessandra.forni@scitec.cnr.it

[4] INFN-National Laboratories of Frascati Via Enrico Fermi 54, 00044 Frascati, Italy; bellucci@lnf.infn.it

* Correspondence: francesca.tessore@unimi.it; Tel.: +39-0250314398

Abstract: Following some previous work by some of us on the second order nonlinear optical (NLO) properties of Zn(II) *meso*-tetraphenylporphyrin (ZnP), fullerene, and ferrocene (Fc) diads and triads, in the present research, we explore the NLO response of some new hybrids with two-dimensional graphene nanoplates (GNP) instead of a zero-dimensional fullerene moiety as the acceptor unit. The experimental data, collected by Electric Field Induced Second Harmonic generation (EFISH) technique in CH_2Cl_2 solution with a 1907 nm incident wavelength, combined with Coupled-Perturbed (CP) and Finite Field (FF) Density Functional Theory (DFT) calculations, show a strongly enhanced contribution of the cubic electronic term $\gamma(-2\omega; \omega, \omega, 0)$, due to the extended π-conjugation of the carbonaceous acceptor moiety.

Keywords: porphyrins; graphene nanoplates; ferrocene; nonlinear optics; hybrid materials

1. Introduction

In the last decades, many materials such as graphene [1–3], fullerene [4–6], and quantum dots [7–9] have attracted attention in the scientific community for their significant nonlinear optical (NLO) properties. In parallel, a huge amount of research has been devoted to the investigation of organic and organometallic chromophores, in which nonlinearity mainly arises from the so-called push–pull architecture, involving a donor and an acceptor moiety bridged by a π-delocalized spacer. Due to their thermal and chemical stability and quite good solubility, porphyrins and their metal complexes are employed in a large variety of fields, ranging from optoelectronics [10,11], catalysis [12–15], sensing technologies [16–20], photovoltaics [21–28], and artificial photosynthesis [29–32]. They have also been long investigated for their second order NLO properties, starting from the pioneering work by Therien [33–35] to some more recent results achieved by some of us [36–40]. Indeed, porphyrins show a very high structural flexibility thanks to the four *meso*, the eight β-pyrrolic, and the two axial positions, which allow a wide variety of chemical functionalizations by playing with the substituents at the periphery of the macrocycle, the nature and the oxidation state of metal center, and the type of axial ligands, for a fine tuning of the optical, electronic, and electrochemical properties in view of an enhanced NLO response.

By using different chemical modifications, several carbonaceous organic moieties such as fullerene, nanotubes, carbon sphere, and graphene [41–48] can efficiently be attached to the porphyrin core to obtain new interesting conjugates [49–52].

In particular, in recent work [52], some of us investigated, using the Electric Field Induced Second Harmonic generation (EFISH) technique, the second order NLO response

in CH_2Cl_2 solution of some dyads (3b(Zn) and (6(Zn)-C60) and triads (10b(Zn)-C60) (Figure S1) formed by the Zn(II) complex of *meso*-tetraphenylporphyrin (ZnP) (Figure S2) with an electron donor ferrocene (Fc), and/or an electron acceptor fullerene (C60) moiety connected to the core in 2 or 2,12 β-pyrrolic position via an ethynylphenyl spacer.

In addition to confirming the possibility for ZnP to act both as an electron acceptor or an electron donor moiety (when connected to electron rich Fc or electron deficient C60, respectively), that study surprisingly highlighted for all the investigated compounds negative EFISH responses. Density Functional Theory (DFT) calculations provided an almost null dipole moment (μ) for 3b(Zn) and μ values in the range 3.5–4.8 D for 6(Zn)-C60 and 10b(Zn)-C60, thus suggesting that these compounds feature a low polarity and, as a consequence, a not negligible third-order contribution to their second order NLO response.

Following these results, this paper represents a part of a larger investigation that we are interested in carrying out on electron donating-accepting multicomponent hybrid systems in search of new promising materials with enhanced nonlinearity. Therefore, in the present research we report and discuss the findings of a combined EFISH and theoretical investigation on the second order NLO properties of some new hybrids, similar to the previous ones, but with two-dimensional graphene nanoplates (GNP) instead of a zero-dimensional C60 moiety, and two ethynylphenyl spacers instead of one (Figure 1). Indeed, the lengthening of the spacer between the ZnP unit and the carbonaceous moiety, and the more π-delocalization of the latter should assure a higher response in comparison to the already studied systems.
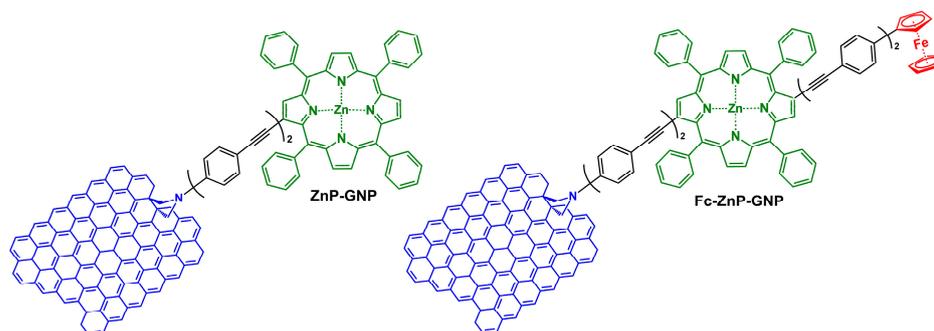
Figure 1. Dyad and triad investigated in this work.

GNP can be described as few layers of graphene, produced in high yields in research-based laboratories. Graphene has been a subject of several investigations by the scientific community, because of its unique physical and chemical properties. However, its application has been hindered by its poor solubility due to the high π–π interlayer attraction energies. This problem can be overcome by the functionalization on the sheet surface by either a covalent or noncovalent method which opens new directions to introduce various organic molecules into graphene sheets [53]. As reported, the π-delocalized electron system of graphene acts as an electron acceptor when connected to a metal porphyrin [54]. Therefore, in our GNP-containing hybrids, push–pull interaction can be envisaged, that may be exploited to boost the second order optical nonlinearity.

2. Materials and Methods

2.1. Materials

The synthesis of the dyad and triad here investigated involves a multi-step process (see Section 3.1). We prepared GNP as reported in [44]. Then, we prepared and characterized Fc-ZnP-CHO, ZnP-GNP, and Fc-ZnP-GNP as reported in [53]. the parent compounds Br-P, Br_2-P, EP_2-CHO, Br-P-CHO, and Fc-P-CHO were also prepared as reported [51,55,56].

We characterized GNP by Scanning Electron Microscopy (SEM) analysis, carried out with a TESCAN VegaII at 10 KV of voltage acceleration with a working distance of 14.67 mm. (Tescan, Brno, Czech Republic).

We recorded the UV–Vis electronic absorption spectra of ZnP-GNP and Fc-ZnP-GNP in CH_2Cl_2 solution at room temperature on a Shimadzu UV 3600 spectrophotometer (Shimadzu Corporation, Kyoto, Japan).

2.2. EFISH Measurements

For the EFISH experiments, we used freshly prepared 10^{-3} M solutions in CH_2Cl_2. We chose a 1.907 µm laser incident wavelength since its second harmonic (at 953 nm) is far enough from the absorption bands of the chromophores in CH_2Cl_2 (see Section 3.3), that is a necessary requirement to avoid any resonance effect on the second order NLO response. We obtained the incident 1.907 µm wavelength by Raman shifting the 1.064 µm emission of a Q-switched Nd:YAG laser in a high pressure hydrogen cell (60 bar). The Maker fringe pattern, typical of the EFISH signal, was obtained through a liquid cell with thick windows in the wedge configuration. In the experiment, we synchronized the incident beam with a DC field applied to the solution, with 60 and 20 ns pulse duration, respectively, in order to break its centrosymmetry. We assumed the NLO response to be real because we neglected the imaginary part, and derived it from the experimental γ_{EFISH} value (Equation (1)):

$$\gamma_{EFISH} = \frac{\mu\beta_\lambda(-2\omega;\omega,\omega)}{5kT} + \gamma(-2\omega;\omega,\omega,0) \tag{1}$$

γ_{EFISH} is the sum of a quadratic dipolar orientational contribution $\mu\beta_\lambda(-2\omega;\omega,\omega)/5$ kT, and of a purely electronic cubic contribution $\gamma(-2\omega;\omega,\omega,0)$. µ is the molecular ground state dipole moment, and β_λ the projection along the dipole moment direction of the vectorial component β_{vec} of the tensorial quadratic hyperpolarizability working with the incident wavelength λ [57,58].

We performed the EFISH experiments at the Department of Chemistry of the University of Milano (Italy), on a prototype apparatus made by SOPRA (Paris, France), recording firstly the second order response of the pure solvent, then the second order response of the chromophore in solution, and finally the second order response of the solvent again. The EFISH values reported in this paper are the average of twelve consecutive measurements performed on the same sample. The uncertainty of the measure is about ±15%, and the experimental EFISH $\beta_{1.907}$ values are defined according to the "phenomenological" convention [59].

2.3. Computational Details

We used the Gaussian16 suite of programs (Revision A.03; Gaussian, Inc.: Wallingford, CT, USA, 2016) to perform DFT calculations. We optimized the molecular geometry with the 6-311G(d) basis set using the PBE0 functional [60,61] in CH_2Cl_2, and we adopted the Polarized Continuum Model in its integral equation formalism (IEFPCM) to describe the solvent effect [62]. We modeled graphene as a single layer of 14 condensed benzene rings and we anchored the porphyrin moiety on the center of the graphene-like system in order to minimize boundary effects. We computed the Second Harmonic Generation (SHG) first, $\beta(-2\omega;\omega,\omega)$, and second, $\gamma(-2\omega;\omega,\omega,0)$, hyperpolarizability tensors by the Coupled Perturbed Kohn–Sham (CPKS) approach and by the Finite Field technique, respectively, at the same frequency of the EFISH experiments (1907 nm). We performed hyperpolarizability calculations at LC-BLYP/6-31G(d) level, in agreement with what was suggested by Wergifosse and Champagne in their thorough investigation on electron correlation effects on the first hyperpolarizability of push–pull π-conjugated systems with polyene and polyyne linkers [63]. We selected a pruned (99,590) grid for computation and use of two-electron integrals and their derivatives. From the full tensors β and γ, we derived the scalar quantities $\beta_\parallel$ and $\gamma_\parallel$, respectively, to have a meaningful comparison with the experimental data. $\beta_\parallel$ corresponds to 3/5 times β_λ, the projection along the dipole moment direction of the vectorial component of the β tensor, that is, $\beta_\parallel = (3/5) \sum_i (\mu_i\beta_i)/\mu$, where $\beta_i = (1/5)\sum_j(\beta_{ijj} + \beta_{jij} + \beta_{jji})$ [64,65]. $\Gamma_\parallel$ is related to the tensor components according

to the following: $\gamma_\parallel$ = (1/15) [3(γ_{xxxx} + γ_{yyyy} + γ_{zzzz}) + 2(γ_{xxyy} + γ_{xxzz} + γ_{yyzz} + γ_{yyxx} + γ_{zzxx} + γ_{zzyy}) + (γ_{xyyx} + γ_{xzzx} + γ_{yzzy} + γ_{yxxy} + γ_{zxxz} + γ_{zyyz})] [64].

3. Results and Discussion

3.1. Synthesis

Although the NLO properties of graphene and porphyrins conjugates have already been investigated, for example by the Z-scan technique [66,67], to the best of our knowledge, the present work is the first EFISH investigation of the second order NLO response of dyad ZnP-GNP and triad Fc-ZnP-GNP. On the other hand, their synthesis has already been reported [53], but since it is not trivial, we wish to recall it (Scheme 1).

We synthesized GNP by a low cost, fast, scalable, and stable fabrication method using a standard 800 W household microwave (MW) oven, developed by some of us [44]. The procedure started with an Asbury Expandable graphite sample (Asbury Carbons, Detroit, MI, USA), where the graphene planes were intercalated with chemical substances such as sulphates and nitrates.

After MW irradiation, the samples were best described by a worm-like morphology with a very large particle area. Using a short ultrasound treatment in isopropyl alcohol, the overall wormlike structures were removed from GNPs. After the treatment, the 2D particles show a lateral dimension of 10 μm and thicknesses < 5 nm, corresponding to several layers of graphene.

Following the GNP synthesis process, we used the new carbon material as the electron acceptor moiety for the formation of dyad ZnP-GNP and triad Fc-ZnP-GNP (Scheme 1).

The synthetic approach that involves the Sonogashira coupling reaction for the formation of carbon–carbon bonds allowed obtaining the desired β-pyrrolic mono and disubstituted compounds.

We chose ethynylphenyl functionalities as molecular bridges, because of their synthetic versatility and their outstanding physicochemical properties. It was previously reported that these linkers assist in a good conduction of the charges due to their high electron density and the extended π-system [65,68–71].

The first step of the synthesis involved bromination of commercially available free-base porphyrin P with N-bromosuccinimide (NBS) to obtain the monobromo derivative Br-P or the dibromo-porphyrin Br_2-P. We carried out the regiospecific antipodal bromination of the macrocycle in 2,12 β-pyrrolic position using a light-induced reaction and NBS in CH_2Cl_2 [72]. Then, the Sonogashira coupling of Br-P or Br_2-P with 1.5 equivalents of 4-[(4′-ethynyl)phenyl]-ethynylbenzaldehyde (EP_2-CHO) afforded derivatives P-CHO and Br-P-CHO in 65 and 36% yield, respectively, after chromatographic purification [56].

For P-CHO, the subsequent step was the insertion of the Zn(II) ion in the cavity of macrocycle, dissolving the free-base in chloroform and adding a 10% excess of a $Zn(OAc)_2$ methanol solution, to afford the corresponding complex ZnP-CHO. Finally, the electron acceptor unit GNP was connected to ZnP-CHO by the Prato–Maggini reaction [73], and we obtained dyad ZnP-GNP.

On the other hand, the preparation of triad Fc-ZnP-GNP involved, before complexation of the core with Zn(II) and the Prato–Maggini reaction, a second Sonogashira coupling between Br-P-CHO and two equivalents of EP_2-Fc, obtaining intermediate Fc-P-CHO in 53% yield [53].

Each intermediate compound of the reaction pathway was characterized and confirmed using mass spectrometry and ^{1}H-NMR spectroscopy (Figures S3–S11 in Supplementary Materials). On the other hand, the final products ZnP-GNP and Fc-ZnP-GNP were characterized by X-ray photoelectron spectroscopy (Figures S12 and S13 in Supplementary Materials) and Raman spectroscopy (Figure S14 in Supplementary Materials).
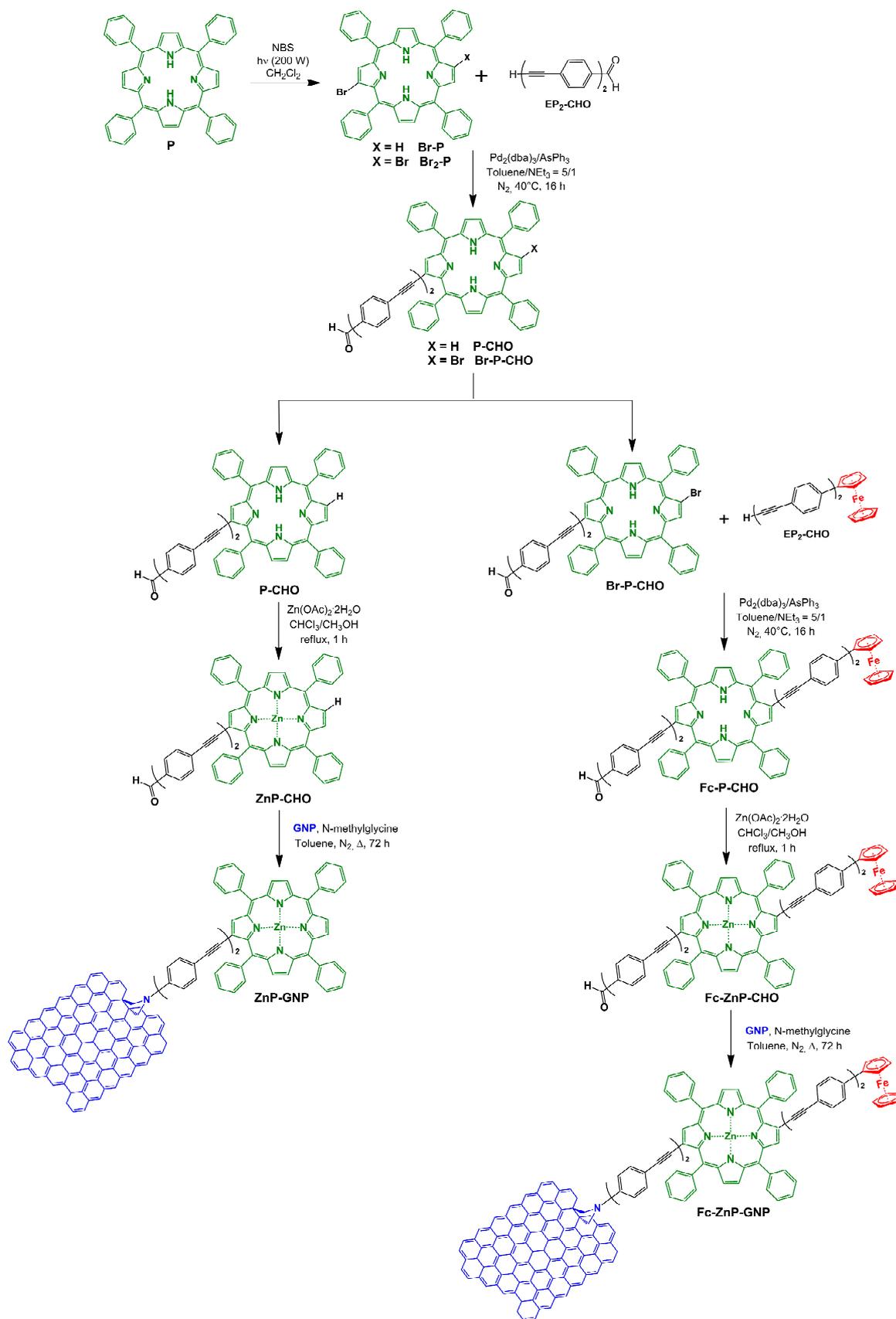
Scheme 1. Synthetic route to the investigated compounds.

3.2. SEM of GNP

We characterized the prepared GNP by SEM analysis (Figure 2). The image shows the micrographs of GNP samples obtained after the irradiation power using a standard 800 W household microwave oven. The SEM micrographs show a smooth surface of the pristine GNP and confirm that the intercalated multilayer graphite had undergone expansion with a good dispersion of the material.
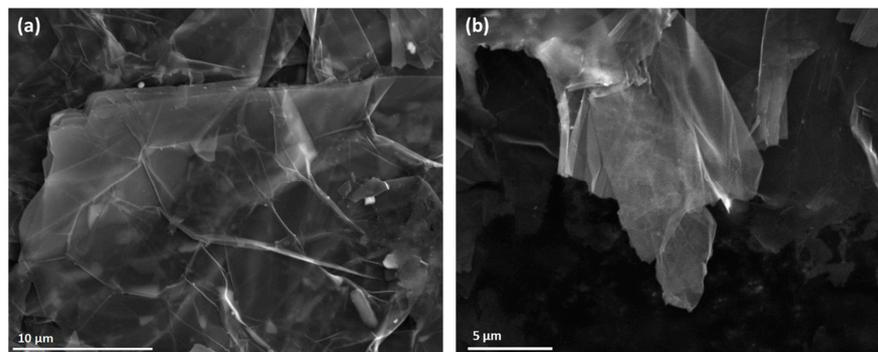
Figure 2. SEM micrographs of GNP sample at different magnifications: (**a**) 10 μm and (**b**) 5 μm.

The 2D particles show a lateral dimension of around 10 μm, corresponding to several layers of graphene (3–7 layers) [39].

3.3. UV–Vis Spectroscopy in Solution

We investigated dyad ZnP-GNP and triad Fc-ZnP-GNP by UV–Vis spectroscopy in CH_2Cl_2 solution (that is, in the same solvent used in the EFISH experiments) to exclude any resonance effect on the second order NLO response, and to see if the replacement of C60 with GNP might have an influence on the electronic properties, since the spectra of reference compounds 6(Zn)-C60 and 10b(Zn)-C60 have been previously reported in this solvent [52].

Figure 3 shows the as-is spectra, together with that of precursor compound Fc-ZnP-CHO (Scheme 1). A synopsis of the UV–Vis data of the investigated compounds and of reference compounds is reported in Table 1.
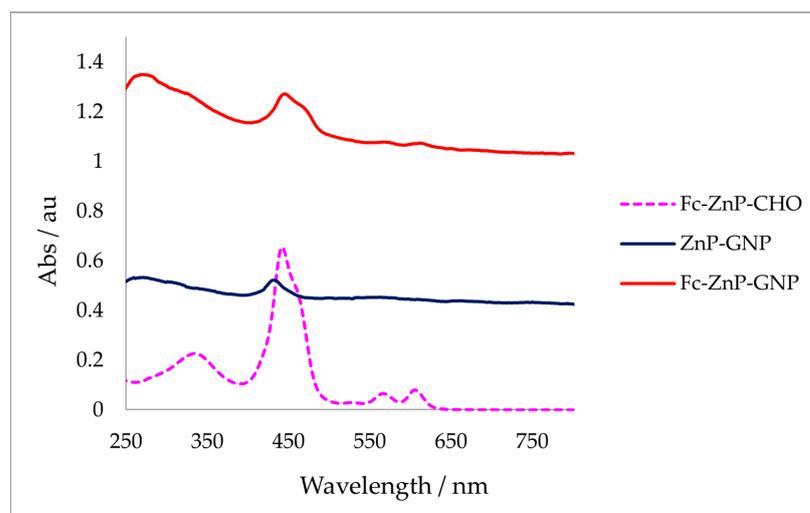
Figure 3. The as-is UV–Vis spectra in CH_2Cl_2 of the investigated compounds and of precursor Fc-ZnP-GNP.

Table 1. Synopsis of the UV–Vis spectroscopic data in CH_2Cl_2 of the GNP-containing hybrids in comparison to C60-containing ones and to precursors Fc-ZnP-CHO and ZnP.

Compound	Soret Band λ_{max} (nm)	Q_α Band λ_{max} (nm)	Q_β Band λ_{max} (nm)
ZnP-GNP	433	nd	nd
Fc-ZnP-GNP	445	567	611
Fc-ZnP-CHO	442	567	605
6(Zn)-C60 [1]	434	560	598
10b(Zn)-C60	438	565	603
ZnP [1]	420	548	589

[1] from ref. [52].

The as-is UV–Vis spectra of ZnP-GNP and Fc-ZnP-GNP are dominated by the significant optical density in the near-IR region, due to the plasmonic resonance of GNP [44], that hampers clearly perceiving the typical pattern of porphyrin metal complexes. Indeed, the spectrum of precursor compound Fc-ZnP-CHO, lacking the GNP unit, shows the classical spectroscopic features expected for a metal porphyrin according to the Gouterman's "four orbital" model [74], that is an intense ($\varepsilon \approx 10^5 \, M^{-1} \, cm^{-1}$) Soret or B band at 400–450 nm, due to a $S_0 \to S_2$ transition, and two less intense ($\varepsilon \approx 10^4 \, M^{-1} \, cm^{-1}$) Q bands at 550–650 nm, ascribed to $S_0 \to S_1$ transitions. For ZnP-GNP only, the Soret band is evident, while the Q bands disappear in the background, so that their wavelength cannot be safely determined, even normalizing the spectrum (Figure S15). On the other hand, in the spectrum of Fc-ZnP-GNP, both the B band and the two Q bands are noticeable, and the former is accompanied by a shoulder at higher wavelengths, which can be ascribed to the Fc unit, since it is present also in the spectrum of Fc-ZnP-CHO.

The covalent bonding of ZnP to GNP in 2 β-pyrrolic position through two ethynylphenyl spacers causes a 13 nm bathochromic shift of the Soret band, supporting the electron withdrawing character of the carbonaceous unit. The further introduction of a Fc moiety in 12 β-pyrrolic antipodal position as in Fc-ZnP-GNP produces an additional 12 nm redshift in comparison to ZnP-GNP. Therefore, not only the interaction with GNP perturbs the electronic state of ZnP [46], but this perturbation is also enhanced in the presence of an electron donor moiety in the antipodal position of the core, suggesting an increased π-delocalization within the system and a more evident push–pull character. Indeed, the functionalization of the electron rich β-pyrrolic position with donor substituents was already reported to be an effective way to enhance the second order NLO properties of porphyrins [75]. The effect of the introduction of GNP on the electronic properties of the investigated hybrids is also confirmed by the 3 and 6 nm redshift experienced by the B and Q_β bands on going from Fc-ZnP-CHO to Fc-ZnP-GNP.

The comparison of the UV–Vis spectra of ZnP-GNP and Fc-ZnP-GNP with those of 6(Zn)-C60, 10b(Zn)-C60, and ZnP (Figures S16 and S17) allows to evaluate both the effect of the replacement of zero-dimensional C60 with two-dimensional GNP as the acceptor part of the push–pull system, and the effect of the presence of two ethynylphenyl linkers instead of one in β-pyrrolic position of the porphyrin core.

Whereas the introduction on ZnP of a C60 moiety bridged by one ethynylphenyl spacer to the core (ZnP → 6(Zn)C60) leads to significant bathochromic shifts of all the absorption bands (14 nm for the B band and 12 and 9 nm for the Q_α abd Q_β bands, respectively), the addition of a further ethynylphenyl unit and the replacement of C60 with GNP appears to have basically no effect on the electronic properties, since only a negligible 1 nm hypsochromic shift of the B band is observed comparing 6(Zn)C60 to ZnP-GNP (Figure S14). C60 and GNP appear, thus, to behave as very similar acceptor groups.

Conversely, the linking of a Fc and a C60 unit in antipodal positions of ZnP (ZnP → 10b(Zn)-C60) produces significant red-shifts of all the absorption bands (18, 17, and 14 nm for the B, Q_α, and Q_β bands, respectively), which are further enhanced by adding a second ethynylphenyl spacer between the core and the donor and acceptor groups, and

replacing C60 with GNP. Indeed, by comparison of the spectrum of 10b(Zn)-C60 with that of Fc-ZnP-GNP, a 7 nm red-shift of the B band is evident, together with 2 and 8 nm red-shifts for the Q_α and Q_β bands.

In summary, the UV–Vis spectroscopic investigation would suggest that a GNP unit linked in the 2 β-pyrrolic position of ZnP perturbs the electronic properties of the core in a way that is similar to C60, thus behaving as an acceptor group of comparable strength. The presence of a Fc moiety in 12 β-pyrrolic antipodal position of the macrocycle appears essential to increase the push–pull character of the system, differently from the insertion of a second ethynylphenyl spacer.

3.4. EFISH and CP-DFT Investigation of the Second Order NLO Properties

We investigated the second order NLO properties of ZnP-GNP and Fc-ZnP-GNP both experimentally by the EFISH technique and theoretically by DFT (see Sections 2.2 and 2.3 for the details). We chose to calculate and discuss $\beta_\parallel$ instead of the spherical averages of the responses (Table S1), since it refers to the projection along the dipole moment direction of the vectorial component of the overall β tensor, which is exactly the figure of merit of the EFISH measure. To better highlight the role of GNP, we also included Fc-ZnP-CHO in our investigation. Figure S18 shows the PBE0/6-311G(d) optimized structures of the three compounds, while Table 2 collects the experimental and theoretical results, together with the data previously reported for the reference compounds with C60 [43].

Table 2. Synopsis of the experimental EFISH and theoretical DFT results on the investigated compounds in comparison to the reference ones.

Compound	μ (D)	γ_{EFISH} ($\times 10^{-36}$ esu)	$\mu\beta_{1907}$ ($\times 10^{-48}$ esu) ($\beta_{1907} \times 10^{-30}$ esu)	$\beta_\parallel$ ($\times 10^{-30}$ esu)	$\mu\beta_\parallel/5\,kT$ ($\times 10^{-36}$ esu)	$\gamma_\parallel$ ($\times 10^{-36}$ esu)	Dipolar vs. Cubic Contribution % [3]
ZnP-GNP	1.23	−3160	−650 (−528) [2]	20	120	−1890	6.3
Fc-ZnP-GNP	1.17	−8800	−1880 (−1607) [2]	9	75	−4388	1.7
Fc-ZnP-CHO	5.31	−4130	−850 (−160) [2]	94	2920	−5484	53
6(Zn)-C60 [1]	4.77	−3470	−720 (−151) [2]	30	696	−1543	45
10b(Zn)-C60 [1]	4.14	−6410	−1330 (−321) [2]	42	845	−3225	26

[1] from ref. [52]. [2] given by $\mu\beta_{1907}/\mu$. [3] given by $[(\mu\beta_\parallel/5\,kT)/\gamma_\parallel] \times 100$.

The experimental γ_{EFISH} and $\mu\beta_{1907}$ values for the GNP-containing hybrids are of the same order of magnitude as those of their C60 counterparts, and, like them, negative [52].

A negative sign of the second order NLO response measured by the EFISH technique can stem from intermolecular interactions or aggregation phenomena that may occur in solution [36,37]. However, as for C60-carrying compounds, as well as ZnP-GNP and Fc-ZnP-GNP, we can safely exclude them, owing to the significant steric hindrance which characterizes A_4 β-pyrrolic mono or disusbstituted Zn(II) porphyrins [37]. Indeed, the dihedral angles between the aryl rings in the four *meso* positions of the core and the mean plane of the macrocycle are in the range 70°–90° (Figure S16), and induce an overall lowering of the molecular flatness.

For 6(Zn)-C60 and 10b(Zn)-C60, some of us reported the negative sign of γ_{EFISH} to be the result of a not-negligible contribution of the electronic third order cubic term $\gamma_0(-2\omega; \omega, \omega, 0)$ to the second order NLO response [52] (see Equation (1)). Indeed, as for other β-pyrrolic mono- and di-substituted Zn(II) porphyrins [39], we observed that in compounds featured by a low polarity, the dipolar orientational contribution $\mu\beta_{1907}(-2\omega; \omega, \omega)/5\,kT$ to γ_{EFISH} becomes less important and is outstripped by

$\gamma_0(-2\omega; \omega, \omega, 0)$, whereas in classical push–pull NLO-phores, this latter can be safely overlooked [76].

The new results on GNP-containing conjugates further support these findings. Indeed, experimental γ_{EFISH} and calculated $\gamma_\parallel$ are almost comparable, at least as order of magnitude, thus confirming the role of third order contributions to the second order NLO response. Moreover, the computed ground state dipole moments (μ) of ZnP-GNP and Fc-ZnP-GNP are very low: 4 and 3.5 times lower than those of reference compounds 6(Zn)-C60 and 10b(Zn)-C60, respectively, and also lower than those of the other β-pyrrolic Zn(II) porphyrins previously studied by some of us [39]. Therefore, from a NLO point of view, we can conclude that GNP behaves as a weaker electron acceptor than C60, and that the dipolar push–pull character of GNP-containing systems decreases in comparison to the C60-containing counterparts, despite the red-shifts of the electronic spectra evidenced by the spectroscopic analysis. Accordingly, the computed $\beta_\parallel$ values for the GNP-containing compounds are from 1.5 to 4.7 times lower than those of the corresponding C60-substituted complexes. On the other hand, their experimental β_{1907} are apparently higher, but these values must be considered carefully since they are the mathematical result of $\mu\beta_{1907}/\mu$ and the μ values of GNP-hybrids are very low, as discussed above. As a general rule, indeed, for the systems under investigation the comparison between β_{1907} and $\beta_\parallel$ is critical, because the former is derived from equation 1 in the assumption of neglecting $\gamma_0 (-2\omega; \omega, \omega, 0)$, that, instead, is crucial.

The role of GNP in the decrease of the dipolar character of the compounds under investigation is confirmed by the fair 5.31 D value of μ obtained for Fc-ZnP-CHO, lacking the GNP unit, which is also higher than those of C60-containing systems and thus leads to a higher value of $\beta_\parallel$. However, even Fc-ZnP-CHO gives rise to a negative γ_{EFISH} value, as expected since the negative $\mu\beta_\parallel/5\ kT$ value is 53% that of $\gamma_\parallel$.

Indeed, in an effort to give at least a qualitative idea of the relationship between the theoretical dipolar and cubic components of the second order NLO response of the investigate compounds, we calculated the ratio between $\mu\beta_\parallel/5\ kT$ and $\gamma_\parallel$ (Table 2, last column). For ZnP-GNP and Fc-ZnP-GNP, the ratio between the calculated dipolar and cubic contribution decreases significantly, becoming less than 10% and supporting the overwhelming role of $\gamma_0(-2\omega; \omega, \omega, 0)$ to γ_{EFISH}. On the other hand, the corresponding C60-containing hybrids and Fc-ZnP-CHO show higher ratios, in agreement with their higher μ and $\beta_\parallel$.

Thus, our combined EFISH and theoretical investigations suggest that the extended π-delocalized structure of GNP enhances the overall polarizability of the GNP-containing hybrids, but without increasing their push–pull character, and therefore leading to chromophores with a not-negligible and significant third order contribution to the second order NLO response.

4. Conclusions

In this work, we integrated an experimental EFISH and a theoretical DFT approach to study the second order NLO properties of two hybrids formed by Zn(II) *meso*-tetraphenyl porphyrin (ZnP), electron acceptor graphene nanoplates (GNP), and electron donor ferrocene (Fc).

The UV–Vis absorption spectra suggested that linking a GNP unit in 2 β-pyrrolic position of ZnP perturbs the electronic properties of the porphyrin core, and that this perturbation is similar to that induced by C60. Moreover, the presence of a Fc moiety in antipodal position of the macrocycle appeared essential to increase the push–pull character of the system, differently from the insertion of a second ethynylphenyl spacer.

EFISH measurements produced for the new GNP-conjugates negative γ_{EFISH} and $\mu\beta_{1907}$ values are comparable to those of C60-containing compounds.

Interestingly, the DFT computed ground state μ for GNP-hybrids was very low, even lower than those of the corresponding compounds with C60, supporting for GNP a less electron acceptor character than C60. The peculiar role of GNP in lowering the μ value

was sustained by the fair μ of Fc-ZnP-CHO, which matched with its higher ratio between the computed dipolar and cubic contributions (53% vs. less than 10%). Nonetheless, since all the investigated compounds, including Fc-ZnP-CHO, showed a negative second order NLO response, we can conclude that γ_{EFISH} is dominated by the negative pure electronic term $\gamma_0(-2\omega; \omega, \omega, 0)$, which overwhelms the dipolar orientational one $\mu\beta_{1907}(-2\omega; \omega, \omega)/5\ kT$. The extended π-delocalized structure of GNP is therefore very efficient in increasing the overall polarizability of the hybrids, without increasing their push–pull character, so that they basically behave as third order chromophores.

Supplementary Materials: The following supporting information can be downloaded at: https://www.mdpi.com/article/10.3390/ma16155427/s1, Figure S1: Dyads and triads already investigated by some of us; Figure S2: Synopsis of chemical structures; Figure S3: FAB spectrum of compound P-CHO using as matrix NBA; Figure S4: ^{1}H-NMR in CDCl$_3$ of compound P-CHO; Figure S5: ^{1}H-NMR in CDCl$_3$ of compound ZnP-CHO; Figure S6: FAB spectrum of compound Br-P-CHO using as matrix NBA: Figure S7: ^{1}H-NMR in CDCl$_3$ of compound Br-P-CHO; Figure S8: MALDI spectrum of compound Fc-P-CHO using as matrix gentisic acid; Figure S9: ^{1}H-NMR in CDCl$_3$ of compound Fc-P-CHO; Figure S10: FAB spectrum of compound Fc-ZnP-CHO using as matrix NBA; Figure S11: ^{1}H NMR in C$_6$D$_6$ of compound Fc-ZnP-CHO; Figure S12: (a) N 1s and (b) Zn 2p$_{3/2,1/2}$ photoemission regions of ZnP-GNP; Figure S13: (a) Fe 2p$_{3/2,1/2}$ and (b) N 1s photoemission regions of Fc-ZnP-GNP; Figure S14: Raman spectrum using a 600 l/mm grating in the spectral range 200–3000 cm^{-1} of Fc-ZnP-GNP; Figure S15: Comparison of the normalized UV-Vis spectra of Fc-ZnP-CHO, ZnP-GNP and Fc-ZnP-GNP in CH$_2$Cl$_2$; Figure S16: Comparison of the normalized UV–Vis spectra of ZnP, 6(Zn)-C60 and ZnP-GNP in CH$_2$Cl$_2$; Figure S17: Comparison of the normalized UV–Vis spectra of ZnP, 10b(Zn)-C60 and Fc-ZnP-GNP in CH$_2$Cl$_2$; Figure S18: PBE0/6-311G(d) optimized structures of (a) ZnP-GNP, (b) Fc-ZnP-GNP and (c) Fc-ZnP-CHO; Table S1: Calculated spherical averages of the responses for the investigated compounds.

Author Contributions: Conceptualization, F.L., F.T. and P.T.; formal analysis, A.F.; investigation, A.L. and S.B.; writing—original draft preparation, F.T. and F.L.; writing—review and editing, F.T., F.L. and P.T.; visualization, C.A. and G.D.C. All authors have read and agreed to the published version of the manuscript.

Institutional Review Board Statement: Not applicable.

Informed Consent Statement: Not applicable.

Data Availability Statement: The data presented in this study are available in the article and in the Supplementary Materials.

Conflicts of Interest: The authors declare no conflict of interest.

References

1. Kumar, V. Linear and Nonlinear Optical Properties of Graphene: A Review. *J. Electron. Mater.* **2021**, *50*, 3773–3799. [CrossRef]
2. You, J.W.; Bongu, S.R.; Bao, Q.; Panoiu, N.C. Nonlinear optical properties and applications of 2D materials. *Theor. Exp. Asp.* **2019**, *8*, 63–97. [CrossRef]
3. Novoselov, K.S.; Geim, A.K.; Morozov, S.V.; Jiang, D.; Zhang, Y.; Dubonos, S.V.; Grigorieva, I.V.; Firsov, A.A. Electric Field Effect in Atomically Thin Carbon Films. *Science* **2004**, *306*, 666–669. [CrossRef] [PubMed]
4. Loboda, O.; Zaleśny, R.; Avramopoulos, A.; Luis, J.-M.; Kirtman, B.; Tagmatarchis, N.; Reis, H.; Papadopoulos, M.G. Linear and Nonlinear Optical Properties of [60]Fullerene Derivatives. *J. Phys. Chem. A* **2009**, *113*, 1159–1170. [CrossRef] [PubMed]
5. Kajzar, F.; Taliani, C.; Zamboni, R.; Rossini, S.; Danieli, R. Nonlinear optical properties of fullerenes. *Synth. Met.* **1996**, *77*, 257–263. [CrossRef]
6. Wang, Y.; Cheng, L.T. Nonlinear optical properties of fullerenes and charge-transfer complexes of fullerenes. *J. Phys. Chem.* **1992**, *96*, 1530–1532. [CrossRef]
7. Limosani, F.; Carcione, R.; Antolini, F. Formation of CdSe quantum dots from single source precursor obtained by thermal and laser treatment. *J. Vac. Sci. Technol. B* **2019**, *38*, 12802–12811. [CrossRef]

8.   Carcione, R.; Limosani, F.; Antolini, F. Cadmium Telluride Nanocomposite Films Formation from Thermal Decomposition of Cadmium Carboxylate Precursor and Their Photoluminescence Shift from Green to Red. *Crystals* **2021**, *11*, 253. [CrossRef]

9.   Antolini, F.; Limosani, F.; Carcione, R. Direct Laser Patterning of CdTe QDs and Their Optical Properties Control through Laser Parameters. *Nanomaterials* **2022**, *12*, 1551. [CrossRef]

10.   Lu, H.; Kobayashi, N. Optically Active Porphyrin and Phthalocyanine Systems. *Chem. Rev.* **2016**, *116*, 6184–6261. [CrossRef]

11.   Collini, E.; Mazzucato, S.; Zerbetto, M.; Ferrante, C.; Bozio, R.; Pizzotti, M.; Tessore, F.; Ugo, R. Large two photon absorption cross section of asymmetric Zn(II) porphyrin complexes substituted in the meso or β pyrrolic position by -C-C≡C-C_6H_4X moieties (X = NMe_2, NO_2). *Chem. Phys. Lett.* **2008**, *454*, 70–74. [CrossRef]

12.   Limosani, F.; Remita, H.; Tagliatesta, P.; Bauer, E.M.; Leoni, A.; Carbone, M. Functionalization of Gold Nanoparticles with Ru-Porphyrin and Their Selectivity in the Oligomerization of Alkynes. *Materials* **2022**, *15*, 1207. [CrossRef]

13.   Bonin, J.; Maurin, A.; Robert, M. Molecular catalysis of the electrochemical and photochemical reduction of CO2 with Fe and Co metal based complexes. Recent advances. *Coord. Chem. Rev.* **2017**, *334*, 184–198. [CrossRef]

14.   Azcarate, I.; Costentin, C.; Robert, M.; Savéant, J.M. Through-Space Charge Interaction Substituent Effects in Molecular Catalysis Leading to the Design of the Most Efficient Catalyst of CO_2-to-CO Electrochemical Conversion. *J. Am. Chem. Soc.* **2016**, *138*, 16639–16644. [CrossRef]

15.   Rao, H.; Schmidt, L.C.; Bonin, J.; Robert, M. Visible-light-driven methane formation from CO_2 with a molecular iron catalyst. *Nature* **2017**, *548*, 74–77. [CrossRef] [PubMed]

16.   Veselov, A.; Thür, C.; Efimov, A.; Guina, M.; Lemmetyinen, H.; Tkachenko, N. Acidity sensor based on porphyrin self-assembled monolayers covalently attached to the surfaces of tapered fibres. *Meas. Sci. Technol.* **2010**, *21*, 115205–115216. [CrossRef]

17.   Garg, K.; Majumder, C.; Gupta, S.K.; Aswal, D.K.; Nayak, S.K.; Chattopadhyay, S. Stable negative differential resistance in porphyrin based σ–π–σ monolayers grafted on silicon. *RSC Adv.* **2015**, *5*, 50234–50244. [CrossRef]

18.   Guo, P.; Zhao, G.; Chen, P.; Lei, B.; Jiang, L.; Zhang, H.; Hu, W.; Liu, M. Porphyrin Nanoassemblies via Surfactant-Assisted Assembly and Single Nanofiber Nanoelectronic Sensors for High-Performance H_2O_2 Vapor Sensing. *ACS Nano* **2014**, *8*, 3402–3411. [CrossRef]

19.   Carbone, M.; Micheli, L.; Limosani, F.; Possanza, F.; Abdallah, Y.; Tagliatesta, P. Ruthenium and manganese metalloporphyrins modified screen-printed electrodes for bio-relevant electroactive targets. *J. Porphyr. Phthalocyanines* **2018**, *22*, 491–500. [CrossRef]

20.   Paolesse, R.; Nardis, S.; Monti, D.; Stefanelli, M.; Di Natale, C. Porphyrinoids for Chemical Sensor Applications. *Chem. Rev.* **2017**, *117*, 2517–2583. [CrossRef]

21.   Li, L.L.; Diau, E.W.G. Porphyrin-sensitized solar cells. *Chem. Soc. Rev.* **2013**, *42*, 291–304. [CrossRef]

22.   Covezzi, A.; Orbelli Biroli, A.; Tessore, F.; Forni, A.; Marinotto, D.; Biagini, P.; Di Carlo, G.; Pizzotti, M. 4D-π-1A type β-substituted Zn^{II}-porphyrins: Ideal green sensitizers for building-integrated photovoltaics. *Chem. Commun.* **2016**, *52*, 12642–12645. [CrossRef] [PubMed]

23.   Di Carlo, G.; Orbelli Biroli, A.; Tessore, F.; Caramori, S.; Pizzotti, M. β-Substituted ZnIIporphyrins as dyes for DSSC: A possible approach to photovoltaic windows. *Coord. Chem. Rev.* **2018**, *358*, 153–177. [CrossRef]

24.   Campbell, W.M.; Burrell, A.K.; Officer, D.L.; Jolley, K.W. Porphyrins as light harvesters in the dye-sensitised TiO2 solar cell. *Coord. Chem. Rev.* **2004**, *248*, 817–833. [CrossRef]

25.   Mathew, S.; Yella, A.; Gao, P.; Humphry-Baker, R.; Curchod, B.F.E.; Ashari-Astani, N.; Tavernelli, I.; Rothlisberger, U.; Nazeeruddin, M.K.; Grätzel, M. Dye-sensitized solar cells with 13% efficiency achieved through the molecular engineering of porphyrin sensitizers. *Nat. Chem.* **2014**, *6*, 242–247. [CrossRef]

26.   Yang, G.; Tang, Y.; Li, X.; Ågren, H.; Xie, Y. Efficient Solar Cells Based on Porphyrin Dyes with Flexible Chains Attached to the Auxiliary Benzothiadiazole Acceptor: Suppression of Dye Aggregation and the Effect of Distortion. *ACS Appl. Mater. Interfaces* **2017**, *9*, 36875–36885. [CrossRef]

27.   Song, H.; Liu, Q.; Xie, Y. Porphyrin-sensitized solar cells: Systematic molecular optimization, coadsorption and cosensitization. *Chem. Commun.* **2018**, *54*, 1811–1824. [CrossRef] [PubMed]

28.   O'Regan, B.; Grätzel, M. A low-cost, high-efficiency solar cell based on dye-sensitized colloidal TiO_2 films. *Nature* **1991**, *353*, 737–740. [CrossRef]

29.   Di Carlo, G.; Orbelli Biroli, A.; Pizzotti, M.; Tessore, F. Efficient sunlight harvesting by A4 β-Pyrrolic Substituted Zn^{II} Porphyrins: A Mini-Review. *Front. Chem.* **2019**, *7*, 177–198. [CrossRef]

30.   Berardi, S.; Caramori, S.; Benazzi, E.; Zabini, N.; Niorettini, A.; Orbelli Biroli, A.; Pizzotti, M.; Tessore, F.; Di Carlo, G. Electronic Properties of Electron-Deficient Zn(II) Porphyrins for HBr Splitting. *Appl. Sci.* **2019**, *9*, 2739. [CrossRef]

31.   Orbelli Biroli, A.; Tessore, F.; Di Carlo, G.; Pizzotti, M.; Benazzi, E.; Gentile, F.; Berardi, S.; Bignozzi, C.A.; Argazzi, R.; Natali, M.; et al. Fluorinated Zn^{II} Porphyrins for Dye-Sensitized Aqueous Photoelectrosynthetic Cells. *ACS Appl. Mater. Interfaces* **2019**, *11*, 32895–32908. [CrossRef] [PubMed]

32.   Materna, K.L.; Jiang, J.; Regan, K.P.; Schmuttenmaer, C.A.; Crabtree, R.H.; Brudvig, G.W. Optimization of Photoanodes for Photocatalytic Water Oxidation by Combining a Heterogenized Iridium Water-Oxidation Catalyst with a High-Potential Porphyrin Photosensitizer. *ChemSusChem* **2017**, *10*, 4526–4534. [CrossRef] [PubMed]

33.   LeCours, S.M.; Guan, H.W.; DiMagno, S.G.; Wang, C.H.; Therien, M.J. Push-pull arylethynyl porphyrins: New chromophores that exhibited large molecular first-order hyperpolarizabilities. *J. Am. Chem. Soc.* **1996**, *118*, 1497–1503. [CrossRef]

34. Karki, L.; Vance, F.W.; Hupp, J.T.; LeCours, S.M.; Therien, M.J. Electronic stark effect studies of a porphyrin-based push-pull chromophore displaying a large first hyperpolarizability: State-specific contributions to β. *J. Am. Chem. Soc.* **1998**, *120*, 2606–2611. [CrossRef]

35. Ray, P.C.; Leszczynski, J. Nonlinear optical properties of highly conjugated push-pull porphyrin aggregates: Role of intermolecular interaction. *Chem. Phys. Lett.* **2006**, *419*, 578–583. [CrossRef]

36. Pizzotti, M.; Tessore, F.; Orbelli Biroli, A.; Ugo, R.; De Angelis, F.; Fantacci, S.; Sgamellotti, A.; Zuccaccia, D.; Macchioni, A. An EFISH, theoretical, and PGSE NMR investigation on the relevant role of aggregation on the second order response in CHCl$_3$ of the push-pull chromophores [5-[[4′-(dimethylamino)phenyl]ethynyl]-15-[(4″-nitrophenyl)ethynyl]-10,20diphenylporphyri. *J. Phys. Chem. C* **2009**, *113*, 11131–11141. [CrossRef]

37. Orbelli Biroli, A.; Tessore, F.; Righetto, S.; Forni, A.; Macchioni, A.; Rocchigiani, L.; Pizzotti, M.; Di Carlo, G. Intriguing Influence of −COOH-Driven Intermolecular Aggregation and Acid-Base Interactions with N,N-Dimethylformamide on the Second-Order Nonlinear-Optical Response of 5,15 Push-Pull Diarylzinc(II) Porphyrinates. *Inorg. Chem.* **2017**, *56*, 6438–6450. [CrossRef] [PubMed]

38. Tessore, F.; Biroli, A.O.; Di Carlo, G.; Pizzotti, M. Porphyrins for Second Order Nonlinear Optics (NLO): An Intriguing History. *Inorganics* **2018**, *6*, 81. [CrossRef]

39. Di Carlo, G.; Pizzotti, M.; Righetto, S.; Forni, A.; Tessore, F. Electric-Field-Induced Second Harmonic Generation Nonlinear Optic Response of A4 β-Pyrrolic-Substituted ZnII Porphyrins: When Cubic Contributions Cannot Be Neglected. *Inorg. Chem.* **2020**, *59*, 7561–7570. [CrossRef]

40. Tessore, F.; Di Carlo, G.; Forni, A.; Righetto, S.; Limosani, F.; Orbelli Biroli, A. Second Order Nonlinear Optical Properties of 4-Styrylpyridines Axially Coordinated to A$_4$ Zn^{II} Porphyrins: A Comparative Experimental and Theoretical Investigation. *Inorganics* **2020**, *8*, 45. [CrossRef]

41. Stegarescu, A.; Cabrera, H.; Budasheva, H.; Soran, M.-L.; Lung, I.; Limosani, F.; Korte, D.; Amati, M.; Borodi, G.; Kacso, I.; et al. Synthesis and Characterization of MWCNT-COOH/Fe3O4 and CNT-COOH/Fe3O4/NiO Nanocomposites: Assessment of Adsorption and Photocatalytic Performance. *Nanomaterials* **2022**, *12*, 3008. [CrossRef] [PubMed]

42. Scarselli, M.; Limosani, F.; Passacantando, M.; D'Orazio, F.; Nardone, M.; Cacciotti, I.; Arduini, F.; Gautron, E.; De Crescenzi, M. Influence of Iron Catalyst in the Carbon Spheres Synthesis for Energy and Electrochemical Applications. *Adv. Mater. Interfaces* **2018**, *5*, 1800070–1800079. [CrossRef]

43. Cinti, S.; Limosani, F.; Scarselli, M.; Arduini, F. Magnetic carbon spheres and their derivatives combined with printed electro-chemical sensors. *Electrochim. Acta* **2018**, *282*, 247–254. [CrossRef]

44. Pierantoni, L.; Mencarelli, D.; Bozzi, M.; Moro, R.; Moscato, S.; Perregrini, L.; Micciulla, F.; Cataldo, A.; Bellucci, S. Broadband Microwave Attenuator Based on Few Layer Graphene Flakes. *IEEE Trans. Microw. Theory Tech.* **2015**, *63*, 2491–2497. [CrossRef]

45. Campidelli, S.; Sooambar, C.; Lozano Diz, E.; Ehli, C.; Guldi, D.M.; Prato, M. Dendrimer-Functionalized Single-Wall Carbon Nanotubes: Synthesis, Characterization, and Photoinduced Electron Transfer. *J. Am. Chem. Soc.* **2006**, *128*, 12544–12552. [CrossRef]

46. Xu, Y.; Liu, Z.; Zhang, X.; Wang, Y.; Tian, J.; Huang, Y.; Ma, Y.; Zhang, X.; Chen, Y. A Graphene Hybrid Material Covalently Functionalized with Porphyrin: Synthesis and Optical Limiting Property. *Adv. Mater.* **2009**, *21*, 1275–1279. [CrossRef]

47. Flavin, K.; Chaur, M.N.; Echegoyen, L.; Giordani, S. Functionalization of Multilayer Fullerenes (Carbon Nano-Onions) using Diazonium Compounds and "Click" Chemistry. *Org. Lett.* **2010**, *12*, 840–843. [CrossRef]

48. Imahori, H.; Sekiguchi, Y.; Kashiwagi, Y.; Sato, T.; Araki, Y.; Ito, O.; Yamada, H.; Fukuzumi, S. Long-Lived Charge-Separated State Generated in a Ferrocene–meso,meso-Linked Porphyrin Trimer–Fullerene Pentad with a High Quantum Yield. *Chem. A Eur. J.* **2004**, *10*, 3184–3196. [CrossRef]

49. Kaur, R.; Possanza, F.; Limosani, F.; Bauroth, S.; Zanoni, R.; Clark, T.; Arrigoni, G.; Tagliatesta, P.; Guldi, D.M. Understanding and Controlling Short- and Long-Range Electron/Charge-Transfer Processes in Electron Donor–Acceptor Conjugates. *J. Am. Chem. Soc.* **2020**, *142*, 7898–7911. [CrossRef]

50. Limosani, F.; Possanza, F.; Ciotta, E.; Pepi, F.; Salvitti, C.; Tagliatesta, P.; Pizzoferrato, R. Synthesis and characterization of two new triads with ferrocene and C60 connected by triple bonds to the beta-positions of *meso*-tetraphenylporphyrin. *J. Porphyr. Phthalocyanines* **2017**, *21*, 364–370. [CrossRef]

51. Possanza, F.; Limosani, F.; Tagliatesta, P.; Zanoni, R.; Scarselli, M.; Ciotta, E.; Pizzoferrato, R. Functionalization of Carbon Spheres with a Porphyrin–Ferrocene Dyad. *ChemPhysChem* **2018**, *19*, 2243–2249. [CrossRef] [PubMed]

52. Limosani, F.; Tessore, F.; Di Carlo, G.; Forni, A.; Tagliatesta, P. Nonlinear Optical Properties of Porphyrin, Fullerene and Ferrocene Hybrid Materials. *Materials* **2021**, *14*, 4404. [CrossRef]

53. Limosani, F.; Kaur, R.; Cataldo, A.; Bellucci, S.; Micciulla, F.; Zanoni, R.; Lembo, A.; Wang, B.; Pizzoferrato, R.; Guldi, D.M.; et al. Designing Cascades of Electron Transfer Processes in Multicomponent Graphene Conjugates. *Angew. Chemie Int. Ed.* **2020**, *59*, 23706–23715. [CrossRef] [PubMed]

54. Georgakilas, V.; Otyepka, M.; Bourlinos, A.B.; Chandra, V.; Kim, N.; Kemp, K.C.; Hobza, P.; Zboril, R.; Kim, K.S. Functionalization of Graphene: Covalent and Non-Covalent Approaches, Derivatives and Applications. *Chem. Rev.* **2012**, *112*, 6156–6214. [CrossRef] [PubMed]

55. Di Carlo, G.; Orbelli Biroli, A.; Pizzotti, M.; Tessore, F.; Trifiletti, V.; Ruffo, R.; Abbotto, A.; Amat, A.; De Angelis, F.; Mussini, P.R. Tetraaryl ZnII Porphyrinates Substituted at β-Pyrrolic Positions as Sensitizers in Dye-Sensitized Solar Cells: A Comparison with meso-Disubstituted Push–Pull ZnII Porphyrinates. *Chem. A Eur. J.* **2013**, *19*, 10723–10740. [CrossRef]

56. Lembo, A.; Tagliatesta, P.; Guldi, D.M.; Wielopolski, M. Porphyrin-b-oligo-ethynylenephenylene-è60]fullerene triads: Synthesis, electrochemical and photophysical characterization of the new porphyrin-oligo-PPE-[60]fullerene systems. *J. Phys. Chem. A* **2009**, *113*, 1779–1793. [CrossRef] [PubMed]

57. Oudar, J.L.; Chemla, D.S. Hyperpolarizabilities of the nitroanilines and their relations to the excited state dipole moment. *J. Chem. Phys.* **1977**, *66*, 2664–2668. [CrossRef]

58. Oudar, J.L. Optical nonlinearities of conjugated molecules. Stilbene derivatives and highly polar aromatic compounds. *J. Chem. Phys.* **1977**, *67*, 446–457. [CrossRef]

59. Willetts, A.; Rice, J.E.; Burland, D.M.; Shelton, D.P. Problems in the comparison of theoretical and experimental hyperpolarizabilities. *J. Chem. Phys.* **1992**, *97*, 7590–7599. [CrossRef]

60. Ernzerhof, M.; Scuseria, G.E. Assessment of the Perdew–Burke–Ernzerhof exchange-correlation functional. *J. Chem. Phys.* **1999**, *110*, 5029–5036. [CrossRef]

61. Adamo, C.; Barone, V. Toward reliable density functional methods without adjustable parameters: The PBE0 model. *J. Chem. Phys.* **1999**, *110*, 6158–6170. [CrossRef]

62. Scalmani, G.; Frisch, M.J. Continuous surface charge polarizable continuum models of solvation. I. General formalism. *J. Chem. Phys.* **2010**, *132*, 114110–114124. [CrossRef] [PubMed]

63. de Wergifosse, M.; Champagne, B. Electron correlation effects on the first hyperpolarizability of push–pull π-conjugated systems. *J. Chem. Phys.* **2011**, *134*, 74113–74125. [CrossRef] [PubMed]

64. Kurtz, H.A.; Dudis, D.S. Quantum Mechanical Methods for Predicting Nonlinear Optical Properties. *Rev. Comput. Chem.* **2007**, *12*, 241–279. [CrossRef]

65. Pielak, K.; Tonnelé, C.; Sanguinet, L.; Cariati, E.; Righetto, S.; Muccioli, L.; Castet, F.; Champagne, B. Dynamical Behavior and Second Harmonic Generation Responses in Acido-Triggered Molecular Switches. *J. Phys. Chem. C* **2018**, *122*, 26160–26168. [CrossRef]

66. Krishna, M.B.M.; Kumar, V.P.; Venkatramaiah, N.; Venkatesan, R.; Rao, D.N. Nonlinear optical properties of covalently linked graphene-metal porphyrin composite materials. *Appl. Phys. Lett.* **2011**, *98*, 81106. [CrossRef]

67. Liu, Z.-B.; Xu, Y.-F.; Zhang, X.-Y.; Zhang, X.-L.; Chen, Y.-S.; Tian, J.-G. Porphyrin and Fullerene Covalently Functionalized Graphene Hybrid Materials with Large Nonlinear Optical Properties. *J. Phys. Chem. B* **2009**, *113*, 9681–9686. [CrossRef]

68. Xiao, X.; Nagahara, L.A.; Rawlett, A.M.; Tao, N. Electrochemical Gate-Controlled Conductance of Single Oligo(phenylene ethynylene)s. *J. Am. Chem. Soc.* **2005**, *127*, 9235–9240. [CrossRef]

69. Lewis, P.A.; Inman, C.E.; Maya, F.; Tour, J.M.; Hutchison, J.E.; Weiss, P.S. Molecular Engineering of the Polarity and Interactions of Molecular Electronic Switches. *J. Am. Chem. Soc.* **2005**, *127*, 17421–17426. [CrossRef]

70. Yu, C.J.; Chong, Y.; Kayyem, J.F.; Gozin, M. Soluble Ferrocene Conjugates for Incorporation into Self-Assembled Monolayers. *J. Org. Chem.* **1999**, *64*, 2070–2079. [CrossRef]

71. Stewart, M.P.; Maya, F.; Kosynkin, D.V.; Dirk, S.M.; Stapleton, J.J.; McGuiness, C.L.; Allara, D.L.; Tour, J.M. Direct Covalent Grafting of Conjugated Molecules onto Si, GaAs, and Pd Surfaces from Aryldiazonium Salts. *J. Am. Chem. Soc.* **2004**, *126*, 370–378. [CrossRef] [PubMed]

72. Di Carlo, G.; Orbelli Biroli, A.; Tessore, F.; Rizzato, S.; Forni, A.; Magnano, G.; Pizzotti, M. Light-Induced Regiospecific Bromination of meso-Tetra(3,5-di-tert-butylphenyl)Porphyrin on 2,12 β-Pyrrolic Positions. *J. Org. Chem.* **2015**, *80*, 4973–4980. [CrossRef] [PubMed]

73. Maggini, M.; Scorrano, G.; Prato, M. Addition of azomethine ylides to C60: Synthesis, characterization, and functionalization of fullerene pyrrolidines. *J. Am. Chem. Soc.* **1993**, *115*, 9798–9799. [CrossRef]

74. Gouterman, M. Spectra of porphyrins. *J. Mol. Spectrosc.* **1961**, *6*, 138–163. [CrossRef]

75. Albert, I.D.L.; Marks, T.J.; Ratner, M.A. Large Molecular Hyperpolarizabilities in "Push-Pull" Porphyrins. Molecular Planarity and Auxiliary Donor—Acceptor Effects. *Chem. Mater.* **1998**, *10*, 753–762. [CrossRef]

76. Planells, M.; Pizzotti, M.; Nichol, G.S.; Tessore, F.; Robertson, N. Effect of torsional twist on 2nd order non-linear optical activity of anthracene and pyrene tricyanofuran derivatives. *Phys. Chem. Chem. Phys.* **2014**, *16*, 23404–23411. [CrossRef] [PubMed]